ACS OMEGA

Article

Cite This: ACS Omega 2018, 3, 9267−9275

http://pubs.acs.org/journal/acsodf

# Reduction-Responsive DNA Duplex Containing $O^6$-Nitrobenzyl-Guanine

Yukiko Hayakawa,[†] Ayaka Banno,[†] Hiroaki Kitagawa,[†] Sayuri Higashi,[†,‡] Yukio Kitade,[†] Aya Shibata,[†] and Masato Ikeda*[,†,‡,§]

[†]Department of Life Science and Chemistry, Graduate School of Natural Science and Technology and [‡]United Graduate School of Drug Discovery and Medical Information Sciences, Gifu University, 1-1 Yanagido, Gifu 501-1193, Japan

[§]Center for Highly Advanced Integration of Nano and Life Sciences, Gifu University (G-CHAIN), Gifu 501-1193, Japan

Supporting Information

**ABSTRACT:** Stimuli-controlled structural transitions of nucleic acids have received growing attentions owing to their potential applications in the fields of chemical and synthetic biology. Here, we describe the development of reduction-responsive deoxyribonucleic acid (DNA) duplexes, in which guanine rings bearing a reduction-responsive cleavable nitrobenzyl (NB) group at the $O^6$ position ($G^{NB}$) are introduced at defined positions. We demonstrate that the artificial NB group can be removed in response to reduction stimulus without the dissociation of the intermolecular duplex structure, which comprises a G-quadruplex forming nucleic acid strand with one $G^{NB}$ and its complementary sequence with one mismatch pair. Meanwhile, another duplex that comprised a G-quadruplex forming nucleic acid strand with two $G^{NB}$ and its complementary sequence with three mismatch pairs exhibited reduction-responsive structural transitions from intermolecular duplex to intramolecular quadruplex. These findings might be useful for the development of DNA architectures endowed with reduction-responsive functions.

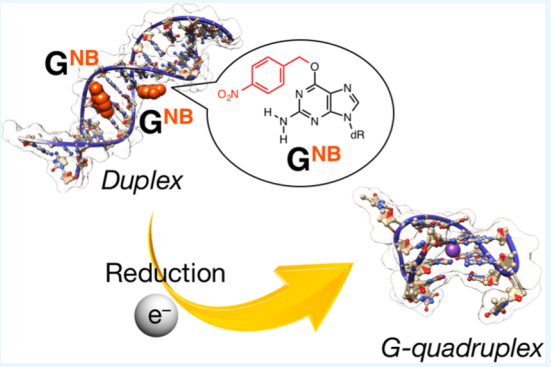


## INTRODUCTION

Stimuli-responsive biomolecules, including nucleic acids, have attracted growing attention because of the possibility to control their functions and processes in biological environments. To this end, photocaged biomolecules have been explored for decades.[1] When introducing photoremovable chemical groups into a target biomolecule, the activities of that biomolecule can be temporarily masked; then, they can be restored by an external stimulus, i.e., photoirradiation, to remove the chemical groups introduced. Moreover, recent progress and deeper understanding of bio-orthogonal chemical reactions have extended the scope of the stimuli: stimuli-triggered release of active biomolecules (decaging) is no longer limited to photostimuli.[2] Some recent interesting examples are the inverse-demand Diels−Alder reaction-triggered decaging to release active proteins, in which tetrazine derivatives can be used as a trigger for the decaging, as described by Chen et al.[3] In addition, Deiters et al. reported a phosphine-mediated Staudinger reduction capable of activating proteins, which are caged via an azido-functionalized amino acid.[4] In those works, xenobiotic, but not seriously toxic, small molecules can trigger the selective decaging to restore active proteins even in living cells. In addition, endogenous compounds, such as reactive oxygen species (e.g., hydrogen peroxide), can be employed to induce the decaging of proteins with phenylboronic acid derivatives.[5] Considering these seminal works on proteins and their progress, chemically caged nucleic acids are not yet sufficiently explored.

Nucleic acids hold inherently important biological activities, for example, even short strands produce RNA interference (RNAi).[6] Moreover, artificially designed or explored functional nucleic acids, such as decoy deoxyribonucleic acid (DNA),[7] aptamers,[8] ribozymes,[9] and DNAzymes,[10] have been actively investigated. Stimuli-responsive control over the structure of nucleic acids would thus set the basis for several bioapplications. Moreover, photocaged nucleic acids have been explored and utilized as tools for biological research, such as light control of transcription, aptamers, antisense activity, and RNAi.[1,11] However, examples of chemically caged nucleic acids and their applications as well as the understanding of their behavior are still rather limited compared to the recent substantial progress on stimuli-responsive proteins. The pioneering work of Micura et al. developed RNAs that contain one or two $O^6$-trichloroethyl-modified guanines ($G^{TCE}$) in their sequences. They are capable of exhibiting zinc-responsive transition in their folding structures accompanied with the recovery of guanine by the removal of the trichloroethyl groups.[12] Recently, Saneyoshi and Ono et al.

Received: May 29, 2018
Accepted: August 1, 2018
Published: August 16, 2018




DOI: 10.1021/acsomega.8b01177
ACS Omega 2018, 3, 9267−9275

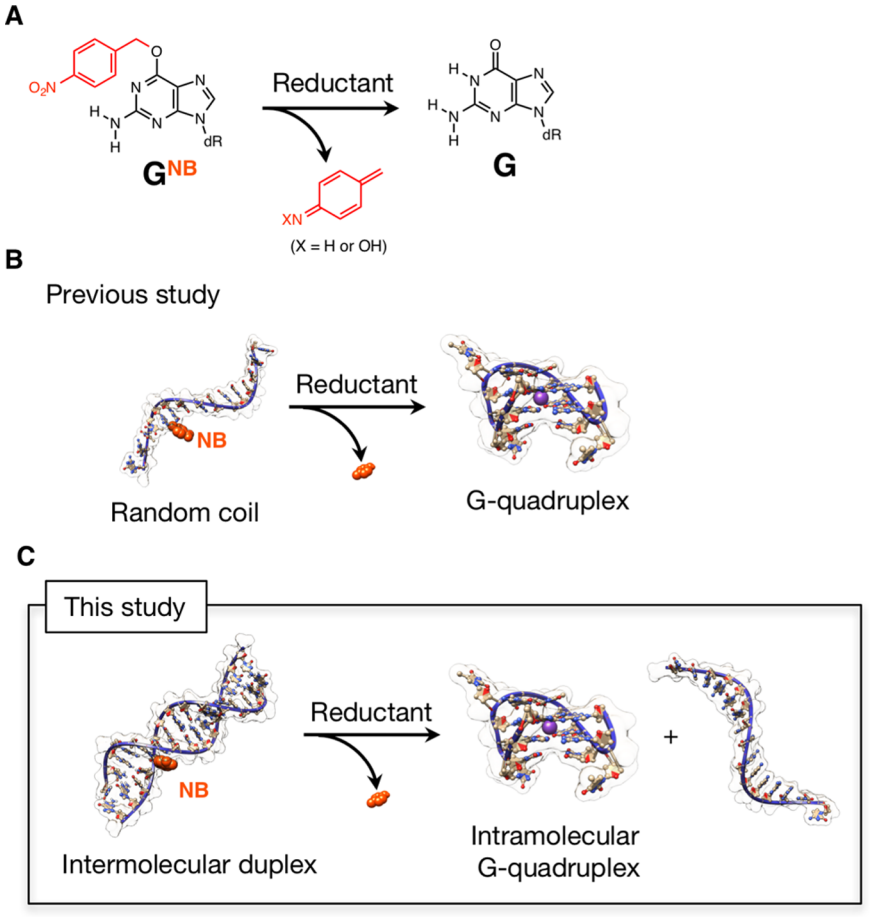


**Figure 1.** (A) Reduction-triggered conversion of $O^6$-nitrobenzyldeoxyguanosine ($G^{NB}$) to deoxyguanosine (G). dR denotes deoxyribose. The typical reductant used in this study is sodium dithionite ($Na_2S_2O_4$). (B, C) Schematic representations of reduction-triggered (B) tertiary structural transition from random coil to intramolecular chair-type antiparallel **TBA** G-quadruplex, reported in the previous study[17] and (C) dissociation of intermolecular duplex to simultaneously form intramolecular **TBA** G-quadruplex with the release of a nearly complementary strand (one $G^{NB}$ is highlighted, see text for the details). The molecular models were constructed using the HyperChem software and visualized with the UCSF Chimera package.[21]

developed a $O^4$-(4-nitrobenzyl)-modified thymine ($T^{NB}$) and investigated the hypoxia(bioreduction)-responsive properties of oligodeoxynucleotides (ODNs) bearing it.[13a] Also, very recently, Morihiro and Obika et al. developed nucleobases bearing 4-boronobenzyl group ($N^{BB}$) and introduced $O^4$-(4-boronobenzyl)-modified thymine into antisense ODNs for hydrogen peroxide-triggered gene silencing.[13b] Not only nucleobases but also other moieties of the nucleic acids, e.g., phosphate diester[14] and ribose,[15] have been target sites for modification with chemically caged groups.[16]

In view of the fact that the guanine exhibits unique structural polymorphs, such as G-quartet, compared with other nucleobases, we previously developed a reduction-responsive guanine ($G^{NB}$, Figure 1A) bearing a nitrobenzyl (NB) group at the $O^6$ position[17] and introduced it into the 5′-end of a G-quadruplex forming DNA (15-mer, 5′-GGTTGGTGTGGTTGG-3′), which is known as thrombin-binding aptamer (**TBA**).[8b] In our previous study,[17] we demonstrated that tertiary structural transition from random coil to intramolecular G-quadruplex (both are single-stranded structures) can be triggered by chemical and enzymatic reductions to convert $G^{NB}$ to G (Figure 1B). Such a stimuli-controlled transition of oligonucleotide tertiary structures might be useful for OFF−ON switching of their functions.

Recently, reduction-responsive biomolecules as well as self-assembled nanomaterials have been attracting increasing attention mostly for cancer-related hypoxia investigations.[18] Conversely, the experience on the selection of aptamers revealed that a significant proportion of DNA aptamers adopt G-quadruplex structures.[19] In addition, polymorphic G-quadruplex structures are involved in telomere DNA structures and their corresponding biological activity.[20] Therefore, stimuli-controlled formation of the G-quadruplex structures might provide potential opportunity to explore OFF−ON switching of target-binding functions or transcription regulation. In this study, we describe the reduction-responsive behavior of intermolecular duplexes, comprising **TBA**s with one or two $G^{NB}$ and their complementary sequences with a specific number of mismatches. **TBA**[8b] was selected as typical and functional G-quadruplex. Also, the relatively short length of **TBA** might be suitable for inducing duplex dissociation in response to a desired stimulus. In particular, we present a sequence design to enable the reduction stimuli-triggered dissociation of such intermolecular duplex to simultaneously release intramolecular **TBA** G-quadruplex (Figure 1C).



DOI: 10.1021/acsomega.8b01177
ACS Omega 2018, 3, 9267−9275

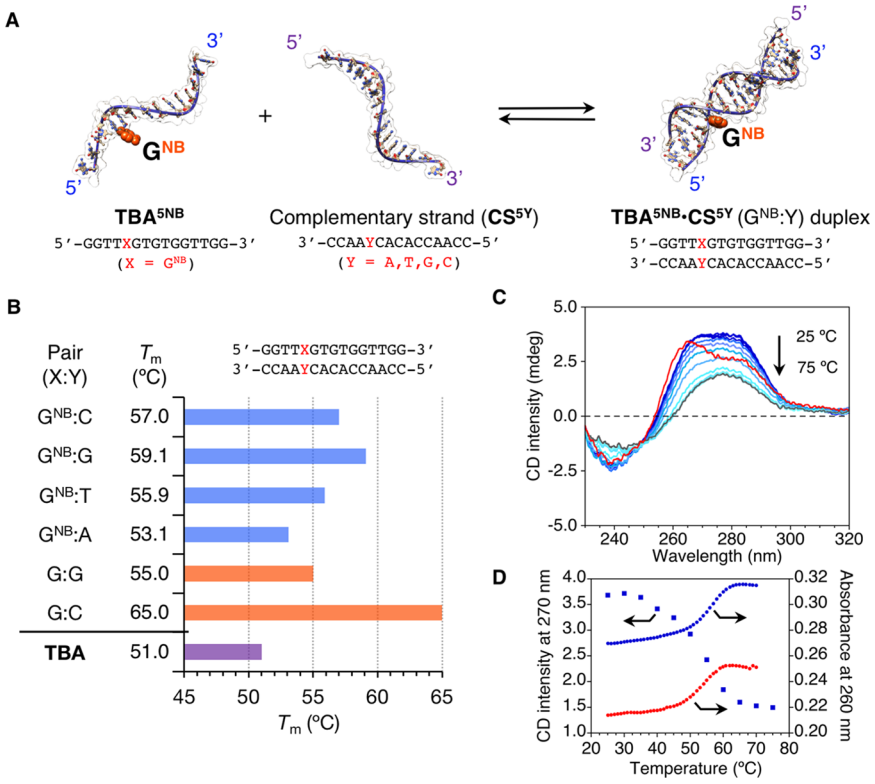


**Figure 2.** (A) Schematic representation of **TBA**$^{5NB}$·**CS**$^{5Y}$ duplexes formation. Duplexes comprise 5′-GGTT**G**$^{NB}$GTGTGGTTGG-3′ (**TBA**$^{5NB}$) and 3′-CCAA**Y**CACACCAACC-5′ (**CS**$^{5Y}$) with different bases incorporated at position Y (A or T or G or C). (B) Thermal stabilities ($T_m$) of **TBA**$^{5NB}$·**CS**$^{5Y}$ duplex and **TBA** G-quadruplex (see Figures S3 and S5). (C) CD spectral changes during thermal melting for **TBA**$^{5NB}$·**CS**$^{5G}$ (blue lines: from 25 to 70 °C at a 5 °C interval, gray line: 75 °C) and CD spectrum of **TBA**·**CS**$^{5C}$ duplex (red line). (D) Representative thermal CD (270 nm, blue squares for **TBA**$^{5NB}$·**CS**$^{5G}$ duplex) and UV (260 nm, blue circles for **TBA**$^{5NB}$·**CS**$^{5G}$, red circles for **TBA**·**CS**$^{5G}$ duplex) melting curves. Conditions: **TBA**$^{5NB}$·**CS**$^{5Y}$ duplex (10 $\mu$M) and **TBA** (10 $\mu$M), 50 mM phosphate buffer (pH 7.6) with 100 mM KCl for (B) and 100 mM *N*-(2-hydroxyethyl)piperazine-*N*′-ethanesulfonic acid (HEPES) (pH 7.0) buffer with 0.1 mM ethylenediaminetetraacetate (EDTA) and 105 mM KCl for (C, D), and 0.1 cm cell length.

## RESULTS AND DISCUSSION

**Sequence Design of Reduction-Responsive G-Quadruplex Forming DNAs Containing One or Two G$^{NB}$.** In this study, we prepared two **TBA**s (15-mer) containing G$^{NB}$: **TBA**$^{5NB}$ (5′-GGTT**G**$^{NB}$GTGTGGTTGG-3′, superscript before NB in "**TBA**$^{5NB}$" is the position from the 5′-end) and **TBA**$^{(5,8)NB2}$ (5′-GGTT**G**$^{NB}$GT**G**$^{NB}$TGGTTGG-3′), according to the previously reported method (see Supporting Information).[17] According to the pioneer studies by Mayer et al., where a photocaged G is incorporated into **TBA** to destabilize or inhibit the formation of the G-quadruplex structure, at least one G from the eight involved in the quadruplex formation has to be replaced with the photocaged G; that is a G at positions 1, 2, 5, 6, 10, 11, 14, or 15 in the sequence shown above.[22] In our previous study, we incorporated a G$^{NB}$ at position 1 (i.e., 5′-end), which enabled almost complete inhibition of the G-quadruplex formation and thus led to the development of a reduction-responsive G-quadruplex forming DNA (**TBA**$^{1NB}$), as shown in Figure 1B. In this study, G was replaced with G$^{NB}$ at position 5 (near the center of the sequence), which is expected to have a substantial effect on the thermodynamic stability of duplexes comprising **TBA**s with G$^{NB}$ and their nearly complementary strands. The incapability of both **TBA**$^{5NB}$ and **TBA**$^{(5,8)NB2}$ to form a G-quadruplex structure and the reduction stimulus-induced formation of a **TBA** G-quadruplex were evident from circular dichroism (CD) spectroscopic measurements, which are similar to those of **TBA**$^{1NB}$ (Figure S6).[17]

**Duplex Formation: TBA with One G$^{NB}$ + Its Nearly Complementary Sequences.** To understand the influence of G$^{NB}$ on the thermodynamic stability of the duplex (Figure 2A), melting temperatures ($T_m$) were measured by means of an ultraviolet (UV) absorption spectroscopy for the nearly complementary sequences 5′-GGTT**X**GTGTGGTTGG-3′ (X = G$^{NB}$, **TBA**$^{5NB}$) and 3′-CCAA**Y**CACACCAACC-5′ (**CS**$^{5Y}$, superscript is the position from the 3′-end). Different bases were incorporated at position **Y** (A or T or G or C) to give a series of **TBA**$^{5NB}$·**CS**$^{5Y}$ (G$^{NB}$:Y) duplexes. As summarized in Figure 2B, the following $T_m$ hierarchy was observed in the order of decreasing stability: G$^{NB}$:G > G$^{NB}$:C > G$^{NB}$:T > G$^{NB}$:A.[23] The four **TBA**$^{5NB}$·**CS**$^{5Y}$ (G$^{NB}$:Y = A or T or G or C) duplexes evidently showed lower thermodynamic stability compared to the perfectly matched native **TBA**·**CS**$^{5C}$ (G:C) duplex ($T_m$ = 65.0 °C). Nonetheless, **TBA**$^{5NB}$·**CS**$^{5G}$ duplex (G$^{NB}$:G, $T_m$ = 59.1 °C), which was the most stable among the four duplexes investigated, was thermodynamically more stable than **TBA**·**CS**$^{5G}$ duplex (G:G, $T_m$ = 55.0 °C) by 4.1 °C ($\Delta T_m$: difference in thermodynamic stability between duplexes with or without NB group).[24] This implies that duplexes bearing a G$^{NB}$:G pair become unstable after the removal of the NB group, which might be promising to induce duplex dissociation in response to a reduction stimulus. The study was thus focused on the G$^{NB}$:G pair.



DOI: 10.1021/acsomega.8b01177
*ACS Omega* 2018, 3, 9267−9275

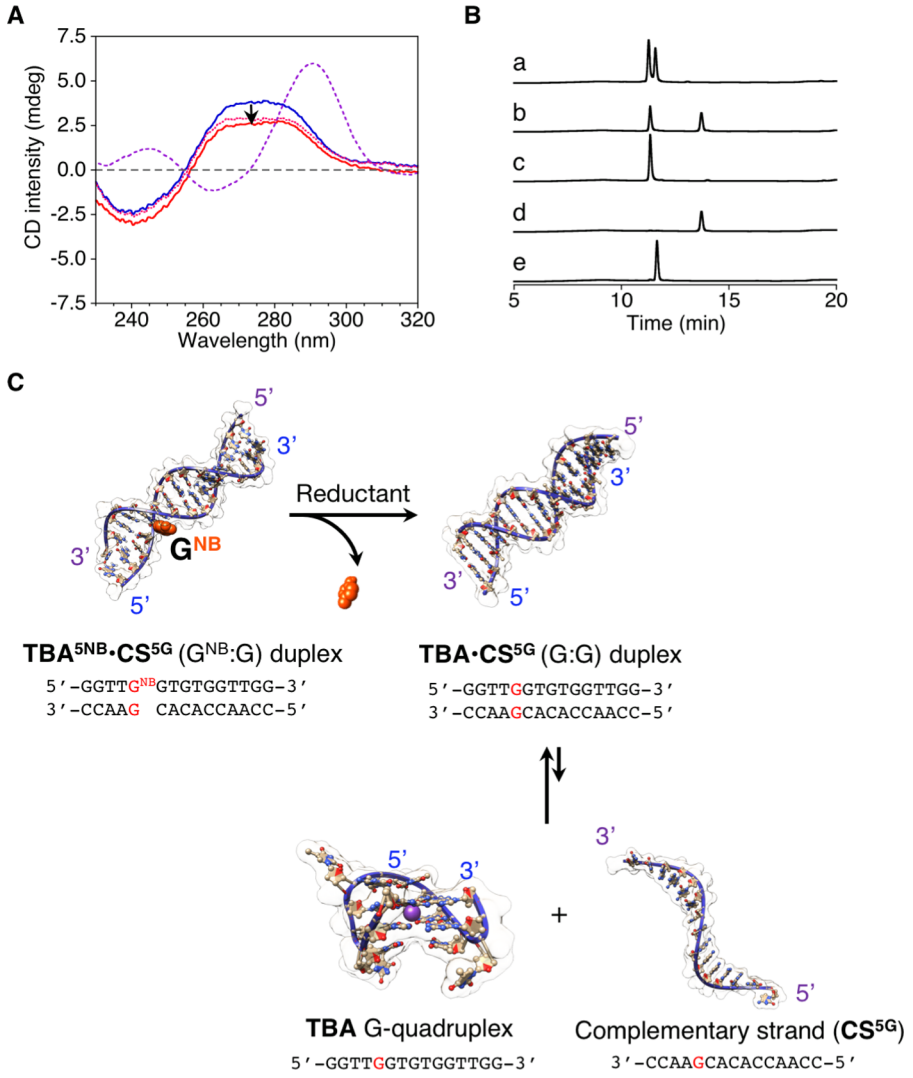


**Figure 3.** (A) CD spectra of the **TBA$^{5NB}$·CS$^{5G}$** duplex before (blue line) and after (red line) the addition of $Na_2S_2O_4$. CD spectrum of a solution containing **TBA** and **CS$^{5G}$** (pink dotted line) and the theoretical sum of the CD spectra of **TBA** and **CS$^{5G}$** (purple dashed line) are also shown. (B) IP RP HPLC chromatograms of (a) **TBA$^{5NB}$·CS$^{5G}$** duplex after the addition of $Na_2S_2O_4$, (b) **TBA$^{5NB}$·CS$^{5G}$** duplex before the addition of $Na_2S_2O_4$, (c) **CS$^{5G}$**, (d) **TBA$^{5NB}$**, and (e) **TBA** (detection at 260 nm). Conditions: **TBA$^{5NB}$·CS$^{5G}$** (10 $\mu$M), $Na_2S_2O_4$/**TBA$^{5NB}$·CS$^{5G}$** = 1050 ([$Na_2S_2O_4$] = 10.5 mM), 100 mM HEPES (pH 7.0) buffer with 0.1 mM EDTA, and 105 mM KCl, 30 °C for (A) CD spectrum and 0.1 cm cell length. (C) Schematic representations showing the reduction-responsive properties of the intermolecular duplex (**TBA$^{5NB}$·CS$^{5G}$** duplex).

The CD spectrum of **TBA$^{5NB}$·CS$^{5G}$** duplex before thermal melting exhibited positive signals centered at 270 nm and negative signals at 240 nm, which can be compared to that of perfectly matched native **TBA·CS$^{5C}$** duplex (Figure 2C). The observed small deviation (i.e., enhanced positive CD intensity at ~280 nm for **TBA$^{5NB}$·CS$^{5G}$** duplex compared to **TBA·CS** duplex) suggests a contribution of the NB group under the chiral environment of a double-stranded helical structure because NB has an absorption band at ~280 nm.[17] CD spectral changes during the thermal melting of **TBA$^{5NB}$·CS$^{5G}$** duplex were characteristic for the double-stranded helical structure of ODNs (a red shift of the zero-crossing wavelength from 257 to 260 nm and a decrease in the intensity of CD signals, Figure 2C). Moreover, both the UV and CD thermal melting experiments of **TBA$^{5NB}$·CS$^{5G}$** duplex gave similar melting curves, as shown in Figure 2D. Also, almost no hysteresis was observed (Figure S4), indicating fast hybridization kinetics of the duplex. Overall, although the exact structure of the **TBA$^{5NB}$·CS$^{5G}$** duplex, i.e., the location or dynamics of NB in the double-stranded helical structure, remains elusive and requires further studies, these results suggest that **TBA$^{5NB}$·CS$^{5G}$** duplex can adopt the standard double-stranded helical structure (most probably a B-form conformation) without significant structural perturbations.

**Reduction Stimuli-Responsive Properties of TBA$^{5NB}$·CS$^{5G}$ Duplex with One G$^{NB}$:G Pair: Reduction-Responsive Duplex Exhibiting No Dissociation.** From thermal denaturation experiments with CD spectroscopy under the $T_m$ measurement conditions similar to the duplexes (Figure S5), the $T_m$ of intramolecular G-quadruplex structure of **TBA** was evaluated as 51.0 °C (Figure 2B, similar to the reported value[25]). Therefore, the thermodynamic stability of the related intermolecular duplexes bearing one G$^{NB}$:G pair and the intramolecular **TBA** G-quadruplex is **TBA$^{5NB}$·CS$^{5G}$** duplex ($T_m$ = 59.1 °C) > **TBA·CS$^{5G}$** duplex ($T_m$ = 55.0 °C) > **TBA** G-quadruplex ($T_m$ = 51.0 °C). This indicates that **TBA·CS$^{5G}$**, which was obtained after the reduction-triggered removal of


DOI: 10.1021/acsomega.8b01177
ACS Omega 2018, 3, 9267−9275

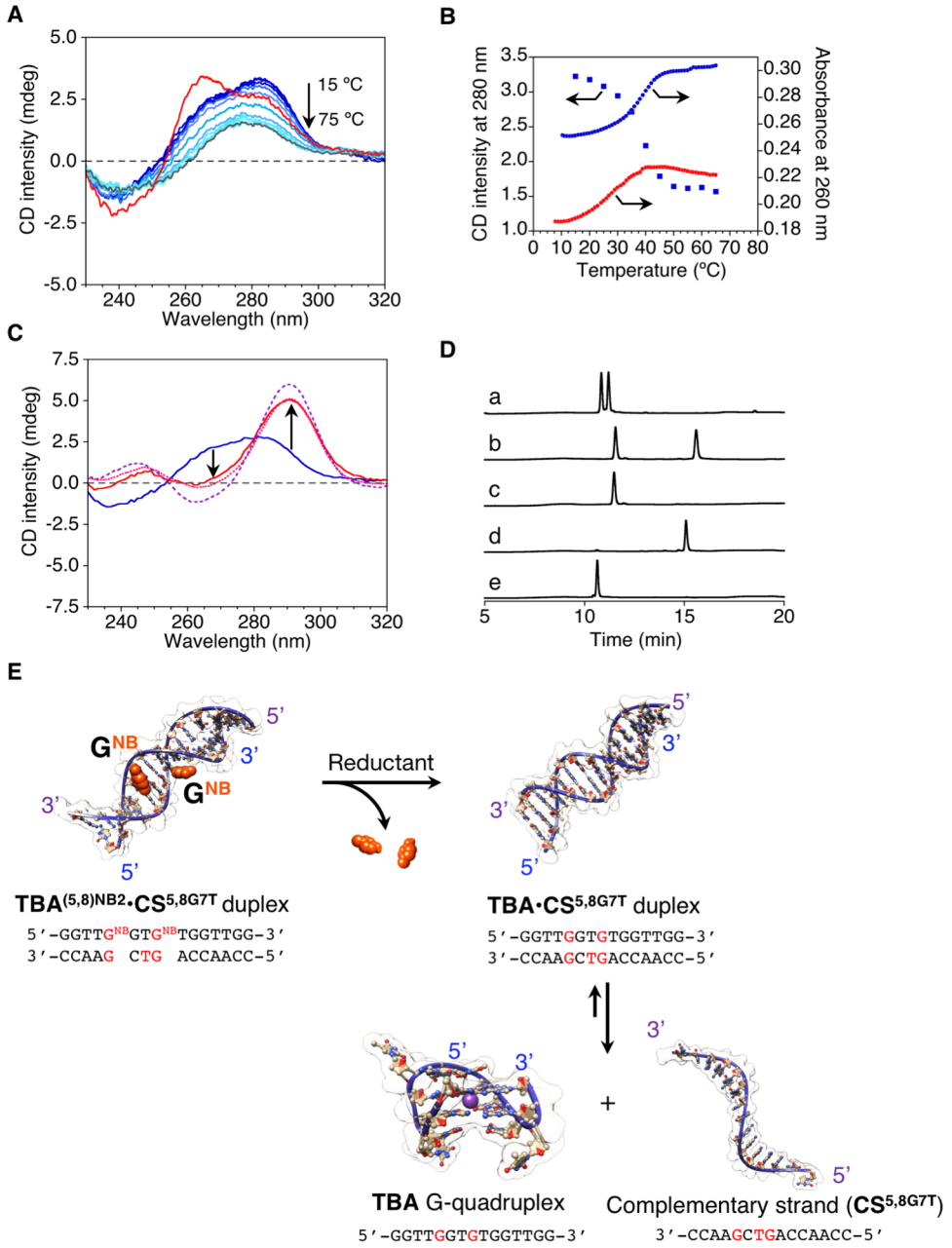


**Figure 4.** (A) CD spectral changes during thermal melting for **TBA**$^{(5,8)NB2}$·**CS**$^{(5,8)G7T}$ (blue lines: from 15 to 70 °C at a 5 °C interval, gray line: 75 °C) and CD spectrum of **TBA**·**CS**$^{5C}$ (red line). (B) Representative thermal CD (280 nm, blue squares for **TBA**$^{(5,8)NB2}$·**CS**$^{(5,8)G7T}$) and UV (260 nm, blue circles for **TBA**$^{(5,8)NB2}$·**CS**$^{(5,8)G7T}$, red circles for **TBA**·**CS**$^{(5,8)G7T}$) melting curves. (C) CD spectra of the **TBA**$^{(5,8)NB2}$·**CS**$^{(5,8)G7T}$ duplex before (blue line) and after (red line) addition of $Na_2S_2O_4$. CD spectrum of a solution containing **TBA** and **CS**$^{(5,8)G7T}$ (pink dotted line) and the theoretical sum of the CD spectra of **TBA** and **CS**$^{(5,8)G7T}$ (purple dashed line) are also shown. The experimental temperature was set at 30 °C. (D) IP RP HPLC chromatograms of (a) **TBA**$^{(5,8)NB2}$·**CS**$^{(5,8)G7T}$ duplex after addition of $Na_2S_2O_4$, (b) **TBA**$^{(5,8)NB2}$·**CS**$^{(5,8)G7T}$ duplex before addition of $Na_2S_2O_4$, (c) **CS**$^{(5,8)G7T}$, (d) **TBA**$^{(5,8)NB2}$, and (e) **TBA** (detection at 260 nm). Conditions: **TBA**$^{(5,8)NB2}$·**CS**$^{(5,8)G7T}$ (10 $\mu$M), $Na_2S_2O_4$/**TBA**$^{(5,8)NB2}$·**CS**$^{(5,8)G7T}$ = 1050 ([$Na_2S_2O_4$] = 10.5 mM), 100 mM HEPES (pH 7.0) buffer with 0.1 mM EDTA and 105 mM KCl, and 0.1 cm cell length. (E) Schematic representations showing reduction-triggered dissociation of double-stranded helix to simultaneously form the G-quadruplex with the release of a nearly complementary strand.

NB from **TBA**$^{5NB}$·**CS**$^{5G}$, is more stable than the intramolecular **TBA** G-quadruplex structure.

To investigate the reduction-responsive conformational change of **TBA**$^{5NB}$·**CS**$^{5G}$ duplex, $Na_2S_2O_4$ was employed as reductant to induce the removal of NB. As shown in Figure 3A, only a small change was observed in the CD spectra of the **TBA**$^{5NB}$·**CS**$^{5G}$ duplex, even after addition of a sufficient amount of $Na_2S_2O_4$ that was determined in our previous study to allow for almost quantitative removal of the NB group. Furthermore, as shown in Figure 3B, the conversion from **TBA**$^{5NB}$ ($t_R$ = 13.7 min) to **TBA** ($t_R$ = 11.6 min) after the addition of $Na_2S_2O_4$ was confirmed by ion-pair reversed-phase high performance liquid chromatography (IP RP HPLC) analyses as well as mass spectra (MS, data not shown). The peaks in the chromatogram were assigned using authentic samples as references or were based on the mass spectra ($t_R$ = 11.3 min for **CS**$^{5G}$). Conversely, in the absence of **CS**$^{5G}$, single-stranded **TBA**$^{5NB}$ showed a sharp increase in the CD signal at



DOI: 10.1021/acsomega.8b01177
ACS Omega 2018, 3, 9267−9275

290 nm after the addition of $Na_2S_2O_4$ under similar conditions (vide supra, Figure S6), which indicates the reduction-responsive folding of **TBA**$^{5NB}$ to form the **TBA** G-quadruplex. These results suggest that the reduction-triggered removal of NB from the **TBA**$^{5NB}$·**CS**$^{5G}$ duplex yielded mostly the **TBA**·**CS**$^{5G}$ duplex with neither duplex dissociation nor **TBA** G-quadruplex formation (Figure 3C).

**Reduction Stimuli-Responsive Properties of the TBA$^{(5,8)NB2}$·CS$^{(5,8)G7T}$ Duplex with Two G$^{NB}$:G Pairs: Transition from Intermolecular Duplex to Intramolecular Quadruplex.** To induce the intermolecular duplex dissociation after reduction-triggered removal of NB and simultaneous intramolecular quadruplex folding (reduction-induced transition from duplex to quadruplex), the minimum requirements would be as follows: (i) the initial sequences of a duplex containing G$^{NB}$ should possess enough thermodynamic stability to maintain intermolecular duplex structure at a given temperature and (ii) thermodynamic stability of the duplex after the removal of NB should become at least lower than that of the intramolecular **TBA** G-quadruplex, hopefully, below the designated temperature. To satisfy these criteria and based on the results mentioned above, the number of G$^{NB}$:G pairs was increased in the initial sequence of the intermolecular duplex. In particular, the G at position 8 in the **TBA** sequence in addition to G at position 5 was replaced with G$^{NB}$ to obtain **TBA**$^{(5,8)NB2}$. Furthermore, based on calculations with the DINAMelt software,[27] one additional mismatch T:T pair was carefully introduced in the middle of the sequence (position 7 from the 5′-end of **TBA**) to modulate the thermodynamic stability of the duplex; i.e., to decrease the stability of the duplex after removal of NB while maintaining the stability of the initial duplex at a given temperature. Thereby, the **TBA**$^{(5,8)NB2}$·**CS**$^{(5,8)G7T}$ duplex was constructed (**TBA**$^{(5,8)NB2}$: 5′-GGTT**G**$^{NB}$GT**G**$^{NB}$TGGTTGG-3′; **CS**$^{(5,8)G7T}$: 3′-CCAAGCT**G**ACCAACC-5′).

From thermal UV denaturation experiments, $T_m$ of the **TBA**$^{(5,8)NB2}$·**CS**$^{(5,8)G7T}$ duplex was evaluated to be 40.8 °C (Figure 4A). In addition, **TBA**$^{(5,8)NB2}$·**CS**$^{(5,8)G7T}$ duplex showed a CD spectrum similar to that of the perfectly matched native **TBA**·**CS** duplex, and the CD melting curve was comparable to the UV melting curve (Figure 4B). Moreover, almost no hysteresis was observed as in the case of **TBA**$^{5NB}$·**CS**$^{5G}$ duplex (Figure S4). These results suggest that the **TBA**$^{(5,8)NB2}$·**CS**$^{(5,8)G7T}$ duplex can also adopt the standard double-stranded helical structure. Notably, $T_m$ of **TBA**·**CS**$^{(5,8)G7T}$ duplex, which should be obtained after the removal of NB from the **TBA**$^{(5,8)NB2}$·**CS**$^{(5,8)G7T}$ duplex, was evaluated to be 27.9 °C according to the UV melting curve (Figure 4B). The large difference in the thermal stability of **TBA**$^{(5,8)NB2}$·**CS**$^{(5,8)G7T}$ duplex before and after the removal of the NB groups compared to that of **TBA**$^{5NB}$·**CS**$^{5G}$ duplex (12.9 °C for **TBA**$^{(5,8)NB2}$·**CS**$^{(5,8)G7T}$ duplex against 4.1 °C for **TBA**$^{5NB}$·**CS**$^{5G}$ duplex as $\Delta T_m$) encouraged us to investigate its reduction-responsive structural transition. On the basis of the $T_m$ values and the melting curves, temperature was set at 30 °C, where **TBA**$^{(5,8)NB2}$·**CS**$^{(5,8)G7T}$ duplex was thermodynamically stable but **TBA**·**CS**$^{(5,8)G7T}$ duplex became unstable.

After the addition of $Na_2S_2O_4$ to the **TBA**$^{(5,8)NB2}$·**CS**$^{(5,8)G7T}$ duplex at 30 °C, a remarkable increase in the CD intensity at 292 nm, which is characteristic of the **TBA** G-quadruplex, was observed within 3 min (Figure 4C). Also, the spectrum after addition of $Na_2S_2O_4$ was almost identical to the mixture of the **TBA** G-quadruplex and **CS**$^{(5,8)G7T}$ and was comparable to a simple theoretical sum of each spectrum (Figure 4C). The difference between the experimental spectrum of the mixture containing **TBA** G-quadruplex and **CS**$^{(5,8)G7T}$ and the theoretical sum of each spectrum implies that the system might not reach to the equilibrium state to provide the complete formation of **TBA** G-quadruplex under these conditions; in other words, **TBA**·**CS**$^{(5,8)G7T}$ duplex and the **TBA** G-quadruplex would be in equilibrium, as depicted in Figure 4E.[26] IP RP HPLC analyses (Figure 4D) as well as mass spectra clearly indicate an almost quantitative conversion from **TBA**$^{(5,8)NB2}$ ($t_R$ = 15.1 min) to **TBA** after addition of $Na_2S_2O_4$. These results support that the dissociation of the **TBA**$^{(5,8)NB2}$·**CS**$^{(5,8)G7T}$ duplex and the simultaneous intramolecular G-quadruplex folding of **TBA** were essentially triggered after addition of the reducing reagent $Na_2S_2O_4$.

Stimuli-controlled transition at high-order structures of nucleic acids is useful for various applications.[28] Nevertheless, single-stranded oligonucleotides are mostly utilized as input signals, which can induce structural transitions following strand exchange reactions via taking advantage of complementary duplex formation, the so called strand displacement, in particular, using the single-stranded toehold motif.[29] In contrast, examples of tertiary structural transition triggered by stimuli other than such single-stranded oligonucleotides are still rather limited. For example, Miyoshi et al. describe that molecular crowding conditions can induce the transition from duplex to quadruplex, which is highly valuable to gain deep understanding of biological events.[30] Very recently, Manderville et al. developed a **TBA** with a fluorescent guanine derivative that allows monitoring structural transitions from duplex to G-quadruplex by fluorescence spectral changes in response to the binding of the modified **TBA** to thrombin.[31] Zhou et al. explored a photoresponsive G-quadruplex binding molecule to modulate G-quadruplex formation in response to light irradiation as external stimulus.[32] In addition, Liu et al. reported pH-driven reversible conformational changes between four- and double-stranded structures on a thin gold surface.[33] This is, to the best of our knowledge, the first example wherein DNA structural transition was induced from duplex to quadruplex in response to reduction stimuli. Considering our previous study, it is reasonably expected that this NB group-based reduction responsiveness can be extended to biomolecule responsiveness after coupling with enzymatic reactions.[34]

## CONCLUSIONS

We successfully constructed reduction-responsive DNA duplexes, in which guanine rings bearing a reduction-responsive cleavable NB group, were introduced at discrete positions and sequences. Moreover, we found that the duplexes exhibit reduction-responsive structural transitions, depending on their sequences. Not only structural transition from intermolecular duplex to intramolecular quadruplex was observed but also the removal of artificial NB groups from intermolecular duplex without its dissociation was demonstrated. Both phenomena are useful for exploring switch functions of biological events, involving DNA duplex and/or quadruplex structures. To explain the behavior of tertiary structures of DNA that contain guanine rings with NB, comprehensive structural studies, such as NMR spectroscopy and X-ray crystallography, may be necessary. Further research along these lines is currently in progress in our laboratory.



DOI: 10.1021/acsomega.8b01177
ACS Omega 2018, 3, 9267−9275

## MATERIALS AND METHODS

Unless stated otherwise, all commercial reagents were used as received. Thrombin-binding aptamer (**TBA**, d-(GGTTGGTGTGGTTGG)) and other oligonucleotides, purified by ion-pair reversed-phase, high-performance liquid chromatography (IP RP HPLC), were synthesized by Fasmac Corp. (Kanagawa, Japan). The concentration of **TBA** was determined at 260 nm and 75 °C using a molar absorption coefficient ($1.46 \times 10^5$ $M^{-1}$ $cm^{-1}$).[25] All water used in the experiments refers to ultrapure water obtained from a Millipore system having a specific resistance of 18 MΩ cm. IP RP HPLC was conducted with a Shimadzu Prominence instrument LC-20AD and SPD-20A equipped with a GL Science Inertsil ODS-3 column (150 mm × 4.6 mm I.D., 5 μm) for analysis and GL Science Inertsil ODS-3 column (150 mm × 10 mm I.D., 5 μm) for purifications in a column oven CTO-20A. Matrix-assisted laser desorption/ionization (MALDI) coupled with time-of-flight (TOF) mass spectra were recorded using a Shimadzu AXIMA-CFR plus mass spectrometer. UV−vis spectra were obtained using a Jasco V-630 or a Shimadzu UV-2450 spectrophotometer.

**Solid-Phase Oligonucleotide Synthesis.** Oligonucleotide synthesis for **TBA**$^{5NB}$ and **TBA**$^{(5,8)NB2}$ was carried out on an NTS H-6 DNA/RNA synthesizer (Nihon Techno Service) using the phosphoramidite method (commercially available phosphoramidite for dG and dC with synthetized dG$^{NB}$ reported previously[17]) at a 1 μmol scale. After cleavage from the solid support, deprotection of bases and phosphates was performed in aqueous ammonia (1.0 mL, 28%) at 55 °C for 12 h. The purification of the "trityl-on" oligonucleotide was carried out on IP RP HPLC ((GL Science Inertsil ODS-3 column (150 mm × 10 mm I.D.)), linear gradient from A/B = 100:0 (A: 0.1 M triethylamine acetate (TEAA) containing 5% acetonitrile, B: acetonitrile) to 50:50 over 30 min was used with a flow rate of 3.0 mL/min, detection wavelength = 260 nm). The purified "trityl-on" oligonucleotide was treated with 80% $CH_3COOH$ for 15 min at 37 °C to remove the dimethoxytrityl residues. The detritylated oligomer was purified by IP RP HPLC ((GL Science Inertsil ODS-3 column (150 mm × 10 mm I.D.)), linear gradient from A/B = 100:0 (A: 0.1 M TEAA containing 5% acetonitrile, B: acetonitrile) to 50:50 over 30 min was used with a flow rate of 3.0 mL/min, detection wavelength = 260 nm). IP RP HPLC charts are shown in Figure S1. The identity of the oligonucleotides **TBA**$^{5NB}$ and **TBA**$^{(5,8)NB2}$ has been established by MALDI-TOF MS (matrix: 3-hydroxypicolinic acid (3-HPA), negative, Figure S2), and the observed molecular weights were in good agreement with their structures: **TBA**$^{5NB}$, calcd for $[M - H]^-$: 4874.1, found: 4876.1 and **TBA**$^{(5,8)NB2}$, calcd. for $[M - H]^-$: 5030.1, found: 5031.3. The oligonucleotide concentrations were determined by UV spectroscopy. The molar extinction coefficient (at 260 nm) ratio of dG$^{NB}$/dG (=1.15) was used to determine the concentrations of **TBA**$^{NB}$ and **TBA**$^{(5,8)NB2}$ by measurements of absorbance (260 nm) at 75 °C.

**Thermal Denaturation Experiments.** *Duplex Sample Preparation.* Hybridization to construct duplexes was accomplished by mixing equal amounts of purified **TBA**s with or without G$^{NB}$ (**TBA**, **TBA**$^{NB}$, or **TBA**$^{(5,8)NB2}$) and their complemented strands with designated number of mismatches to a final concentration of 100 μM in (A) 10 mM phosphate buffer (pH 7.6) containing 100 mM KCl or (B) 100 mM HEPES buffer (pH 7.0) containing 105 mM KCl. The samples were heated at 95 °C for 5 min followed by cooling to room temperature over a period of approximately 1 h. The samples were then stored at 4 °C until experiments were accomplished.

*Ultraviolet (UV) Melting Experiments.* UV melting experiments were carried out on a Jasco V-630 spectrometer equipped with a programmable temperature-control unit (Jasco ETCS-761) using a 0.1 cm quartz cell unless otherwise noted. The melting temperatures ($T_m$s) were determined from the maximum in the first derivatives of the melting curves (absorbance at 260 nm against temperature, 0.5 °C/min). Oligonucleotides were diluted at a final concentration of 10 μM in aqueous buffers.

*Circular Dichroism (CD) Spectral Measurements and Melting Experiments.* CD experiments were carried out on a Jasco J-820 spectropolarimeter equipped with a programmable temperature-control unit (Julabo HP-4) using a 0.1 cm quartz cell unless otherwise noted. CD spectra were obtained by using a 1 nm slit width and a scanning step of 0.1 nm from 320 to 230 nm. Each spectrum was an average of eight scans with the buffer background subtracted. The melting temperatures ($T_m$s) were determined from the maximum in the first derivatives of the melting curves (CD intensity at 292 nm against temperature, 1.0 °C/min).

**Monitoring Reduction-Responsive Structural Change by CD and IP RP HPLC.** Stock solution of oligonucleotide duplexes was diluted with an aqueous buffer to afford solutions containing oligonucleotide duplexes (10 μM). The reductant ($Na_2S_2O_4$) was then added to adjust ca. 10 mM as the final concentrations in the mixture. After incubation at designated temperature (25, 30, or 35 °C), CD spectral changes were measured under the conditions mentioned above. Also, the reaction mixture was subjected to IP RP HPLC analysis (GL Science Inertsil ODS-3 column (150 mm × 4.6 mm I.D., 5 μm), linear gradient from A/B = 100:0 (A: 0.1 M TEAA containing 5% acetonitrile, B: acetonitrile) to 50:50 over 30 min was used with a flow rate of 1.0 mL/min, detection wavelength = 260 nm, column oven temperature = 40 °C). The identity of the starting oligonucleotides (**TBA**$^{5NB}$, **TBA**$^{(5,8)NB2}$) and the desired reduction product (**TBA**) were established by comparing the retention time of authentic standard as well as MALDI-TOF MS spectra. Experiment was repeated in at least duplicates.

## ASSOCIATED CONTENT

### Supporting Information

The Supporting Information is available free of charge on the ACS Publications website at DOI: 10.1021/acsomega.8b01177.

Figures showing characterization of oligonucleotides; thermal denaturation experiments; and reduction-responsive property (Figures S1−S8) (PDF)

## AUTHOR INFORMATION

### Corresponding Author

*E-mail: m_ikeda@gifu-u.ac.jp.

### ORCID

Masato Ikeda: 0000-0003-4097-8292

### Notes

The authors declare no competing financial interest.



DOI: 10.1021/acsomega.8b01177
ACS Omega 2018, 3, 9267−9275

## ■ ACKNOWLEDGMENTS

This work was supported in part by a Grant-in-Aid for Scientific Research (B) (M.I., No. 15H03836) of the Japan Society for the Promotion of Science. Financial supports from Mochida Memorial Foundation for Medical and Pharmaceutical Research and Daiichi Sankyo Foundation of Life Science to M.I. are also acknowledged. We acknowledge Division of Instrumental Analysis, Life Science Research Centre, Gifu University for the maintenance of the instruments and kind support (especially, Prof. Yasunori Oumi, Prof. Shigeo Takashima, Dr. Yoshiharu Sawada, Yoshiko Wakihara and Kayoko Toyoshi). The authors would like to thank Enago (www.enago.jp) for the English language review.

## ■ REFERENCES

(1) For recent reviews (a) Klán, P.; Šolomek, T.; Bochet, C. G.; Blanc, A.; Givens, R.; Rubina, M.; Popik, V.; Kostiko, A.; Wirz, J. Photoremovable protecting groups in chemistry and biology: reaction mechanisms and efficacy. *Chem. Rev.* **2013**, *113*, 119−191. (b) Brieke, C.; Rohrbach, F.; Gottschalk, A.; Mayer, G.; Heckel, A. Light-controlled tools. *Angew. Chem., Int. Ed.* **2012**, *51*, 8446−8476. (c) Yu, H.; Li, J.; Wu, D.; Qiua, Z.; Zhang, Y. Chemistry and biological applications of photo-labile organic molecules. *Chem. Soc. Rev.* **2010**, *39*, 464−473. (d) Lee, H.-M.; Larson, D. R.; Lawrence, D. S. Illuminating the chemistry of life: design, synthesis, and applications of "caged" and related photoresponsive compounds. *ACS Chem. Biol.* **2009**, *4*, 409−427. (e) Ellis-Davies, G. C. R. Caged compounds: photorelease technology for control of cellular chemistry and physiology. *Nat. Methods* **2007**, *4*, 619−628.

(2) For recent reviews (a) Li, J.; Chem, P. R. Development and application of bond cleavage reactions in bioorthogonal chemistry. *Nat. Chem. Biol.* **2016**, *12*, 129−137. (b) Völker, T.; Meggers, E. Transition-metal-mediated uncaging in living human cells—an emerging alternative to photolabile protecting groups. *Curr. Opin. Chem. Biol.* **2015**, *25*, 48−54.

(3) (a) Li, J.; Jia, S.; Chen, P. R. Diels-Alder reaction-triggered bioorthogonal protein decaging in living cells. *Nat. Chem. Biol.* **2014**, *10*, 1003−1005. (b) Fan, X.; Ge, Y.; Lin, F.; Yang, Y.; Zhang, G.; Ngai, W. S. C.; Lin, Z.; Zheng, S.; Wang, J.; Zhao, J.; Li, J.; Chen, P. R. Optimized tetrazine derivatives for rapid bioorthogonal decaging in living cells. *Angew. Chem., Int. Ed.* **2016**, *55*, 14046−14050.

(4) Luo, J.; Liu, Q.; Morihiro, K.; Deiters, A. Small-molecule control of protein function through Staudinger reduction. *Nat. Chem.* **2016**, *8*, 1027−1034.

(5) (a) Chen, Z.-j.; Tian, Z.; Kallio, K.; Oleson, A. L.; Ji, A.; Borchardt, D.; Jian, D.-e.; Remington, S. J.; Ai, H.-w. The N−B interaction through a water bridge: understanding the chemoselectivity of a fluorescent protein based probe for peroxynitrite. *J. Am. Chem. Soc.* **2016**, *138*, 4900−4907. (b) Hoang, T. T.; Smith, T. P.; Raines, R. T. A. Boronic acid conjugate of angiogenin that shows ROS-responsive neuroprotective activity. *Angew. Chem., Int. Ed.* **2017**, *56*, 2619−2622. (c) Wang, M.; Sun, S.; Neufeld, C. I.; Perez-Ramirez, B.; Xu, Q. Reactive oxygen species-responsive protein modification and its intracellular delivery for targeted cancer therapy. *Angew. Chem., Int. Ed.* **2014**, *53*, 13444−13448. (d) Brustad, E.; Bushey, M. L.; Lee, J. W.; Groff, D.; Liu, W.; Schultz, P. G. A genetically encoded boronate-containing amino acid. *Angew. Chem., Int. Ed.* **2008**, *47*, 8220−8223.

(6) (a) Elbashir, S. M.; Harborth, J.; Lendeckel, W.; Yalcin, A.; Weber, K.; Tuschl, T. Duplexes of 21-nucleotide RNAs mediate RNA interference in cultured mammalian cells. *Nature* **2001**, *411*, 494−498. (b) Hannon, G. J. RNA interference. *Nature* **2002**, *418*, 244−251.

(7) (a) Morishita, R.; Sugimoto, T.; Aoki, M.; Kida, I.; Tomita, N.; Moriguchi, A.; Maeda, K.; Sawa, Y.; Kaneda, Y.; Higaki, J.; Ogihara, T. In vivo transfection of cis element "decoy" against nuclear factor-kappaB binding site prevents myocardial infarction. *Nat. Med.* **1997**, *3*, 894−899. (b) Bielinska, A.; Shivdasani, R. A.; Zhang, L. Q.; Nabel, G. J. Regulation of gene expression with double-stranded phosphorothioate oligonucleotides. *Science* **1990**, *250*, 997−1000.

(8) (a) Ellington, A. D.; Szostak, J. W. In vitro selection of RNA molecules that bind specific ligands. *Nature* **1990**, *346*, 818−822. (b) Bock, L. C.; Griffin, L. C.; Latham, J. A.; Vermaas, E. H.; Toole, J. J. Selection of single-stranded DNA molecules that bind and inhibit human thrombin. *Nature* **1992**, *355*, 564−566. For recent review (c) Poolsup, S.; Kim, C.-Y. Therapeutic applications of synthetic nucleic acid aptamers. *Curr. Opin. Biotechnol.* **2017**, *48*, 180−186.

(9) (a) Kruger, K.; Grabowski, P. J.; Zaug, A. J.; Sands, J.; Gottschling, D. E.; Cech, T. R. Self-splicing RNA: autoexcision and autocyclization of the ribosomal RNA intervening sequence of Tetrahymena. *Cell* **1982**, *31*, 147−157. (b) Guerrier-Takada, C.; Gardiner, K.; Marsh, T.; Pace, N.; Altman, S. The RNA moiety of ribonuclease P is the catalytic subunit of the enzyme. *Cell* **1983**, *35*, 849−857. (c) Robertson, D. L.; Joyce, G. F. Selection in vitro of an RNA enzyme that specifically cleaves single-stranded DNA. *Nature* **1990**, *344*, 467−468. For review. (d) Hammann, C.; Luptak, A.; Perreault, J.; de la Pena, M. The ubiquitous hammerhead ribozyme. *RNA* **2012**, *18*, 871−885.

(10) (a) Ponce-Salvatierra, A.; Wawrzyniak-Turek, K.; Steuerwald, U.; Höbartner, C.; Pena, V. Crystal structure of a DNA catalyst. *Nature* **2016**, *529*, 231−234. (b) Breaker, R. R.; Joyce, G. F. A DNA enzyme that cleaves RNA. *Chem. Biol.* **1994**, *1*, 223−229. For review (c) Silverman, S. K. Catalytic DNA (deoxyribozymes) for synthetic applications—current abilities and future prospects. *Chem. Commun.* **2008**, 3467−3485.

(11) For review (a) Liu, Q.; Deiters, A. Optochemical control of deoxyoligonucleotide function via a nucleobase-caging approach. *Acc. Chem. Res.* **2014**, *47*, 45−55. (b) Tang, X.; Dmochowski, I. J. Regulating gene expression with light-activated oligonucleotides. *Mol. BioSyst.* **2007**, *3*, 100−110.

(12) Höbartner, C.; Mittendorfer, H.; Breuker, K.; Micura, R. Triggering of RNA Secondary structures by a functionalized nucleobase. *Angew. Chem., Int. Ed.* **2004**, *43*, 3922−3925.

(13) (a) Saneyoshi, H.; Hiyoshi, Y.; Iketani, K.; Kondo, K.; Ono, A. Bioreductive deprotection of 4-nitrobenzyl group on thymine base in oligonucleotides for the activation of duplex formation. *Bioorg. Med. Chem. Lett.* **2015**, *25*, 5632−5635. (b) Mori, S.; Morihiro, K.; Okuda, T.; Kasahara, Y.; Obika, S. Hydrogen peroxide-triggered gene silencing in mammalian cells through boronated antisense oligonucleotides. *Chem. Sci.* **2018**, *9*, 1112−1118.

(14) (a) Meade, B. R.; Gogoi, K.; Hamil, A. S.; Palm-Apergi, C.; van den Berg, A.; Hagopian, J. C.; Springer, A. D.; Eguchi, A.; Kacsinta, A. D.; Dowdy, C. F.; Presente, A.; Lönn, P.; Kaulich, M.; Yoshioka, N.; Gros, E.; Cui, X.-S.; Dowdy, S. F. Efficient delivery of RNAi prodrugs containing reversible charge-neutralizing phosphotriester backbone modifications. *Nat. Biotechnol.* **2014**, *32*, 1256−1261. (b) Saneyoshi, H.; Ono, A. Development of protecting groups for prodrug-type oligonucleotide medicines. *Chem. Pharm. Bull.* **2018**, *66*, 147−154.

(15) Ochi, Y.; Nakagawa, O.; Sakaguchi, K.; Wada, S.-i.; Urata, H. A post-synthetic approach for the synthesis of 2'-*O*-methyldithiomethyl-modified oligonucleotides responsive to a reducing environment. *Chem. Commun.* **2013**, *49*, 7620−7622.

(16) For review Ikeda, M.; Kabumoto, M. Chemically caged nucleic acids. *Chem. Lett.* **2017**, *46*, 634−640.

(17) Ikeda, M.; Kamimura, M.; Hayakawa, Y.; Shibata, A.; Kitade, Y. Reduction-responsive guanine incorporated into G-quadruplex-forming DNA. *ChemBioChem* **2016**, *17*, 1304−1307.

(18) (a) Wilson, W. R.; Hay, M. P. Targeting hypoxia in cancer therapy. *Nat. Rev. Cancer* **2011**, *11*, 393−410. (b) Thambi, T.; Park, J. H.; Lee, D. S. Hypoxia-responsive nanocarriers for cancer imaging and therapy: recent approaches and future perspectives. *Chem. Commun.* **2016**, *52*, 8492−8500.

(19) Platella, C.; Riccardi, C.; Montesarchio, D.; Roviello, G. N.; Musumeci, D. G-quadruplex-based aptamers against protein targets in therapy and diagnostics. *Biochim. Biophys. Acta, Gen. Subj.* **2017**, *1861*, 1429−1447.



DOI: 10.1021/acsomega.8b01177
*ACS Omega* 2018, 3, 9267−9275

(20) (a) Siddiqui-Jain, A.; Grand, C. L.; Bearss, D. J.; Hurley, L. H. Direct evidence for a G-quadruplex in a promoter region and its targeting with a small molecule to repress c-*MYC* transcription. *Proc. Natl. Acad. Sci. U.S.A.* **2002**, *99*, 11593−11598. (b) Biffi, G.; Tannahill, D.; McCafferty, J.; Balasubramanian, S. Quantitative visualization of DNA G-quadruplex structures in human cells. *Nat. Chem.* **2013**, *5*, 182−186. (c) Bochman, M. L.; Paeschke, K.; Zakian, V. A. DNA secondary structures: stability and function of G-quadruplex structures. *Nat. Rev. Genet.* **2012**, *13*, 770−780.

(21) Chimera is developed by the Resource for Biocomputing, Visualization, and Informatics at the University of California, San Francisco (supported by NIGMS P41-GM103311). Pettersen, E. F.; Goddard, T. D.; Huang, C. C.; Couch, G. S.; Greenblatt, D. M.; Meng, E. C.; Ferrin, T. E. UCSF Chimera–a visualization system for exploratory research and analysis. *J. Comput. Chem.* **2004**, *25*, 1605−1612.

(22) Mayer, G.; Kröck, L.; Mikat, V.; Engeser, M.; Heckel, A. Light-induced formation of G-quadruplex DNA secondary structures. *ChemBioChem* **2005**, *6*, 1966−1970.

(23) This is the similar order of decreasing thermal stability reported previously for $O^6$-benzylguanine ($G^B$) paired with the canonical bases in double-stranded helical structures of ODNs. $G^B$ as well as $O^6$-methylguanine ($G^{Me}$) is frequently found as $O^6$-alkylguanine lesions. (a) Gong, J.; Sturla, S. J. A synthetic nucleoside probe that discerns a DNA adduct from unmodified DNA. *J. Am. Chem. Soc.* **2007**, *129*, 4882−4883. (b) Gaffney, B. L.; Jones, R. A. Thermodynamic comparison of the base pairs formed by the carcinogenic lesion $O^6$-methylguanine with reference both to Watson-Crick pairs and to mismatched pairs. *Biochemistry* **1989**, *28*, 5881−5889.

(24) The phosphate buffer was used for the evaluation of $T_m$ due to temperature dependent p$K_a$ of HEPES. The HEPES buffer was used for the other experiments in relationship to our previous study. Nevertheless, there was no significant difference in thermal melting behaviors in this study as far as we tested.

(25) Kankia, B. I.; Marky, L. A. Folding of the thrombin aptamer into a G-quadruplex with $Sr^{2+}$: stability, heat, and hydration. *J. Am. Chem. Soc.* **2001**, *123*, 10799−10804.

(26) CD spectrum of the mixture containing **TBA** G-quadruplex and $\mathbf{CS}^{(5,8)\mathbf{G7T}}$ became almost identical to the theoretical sum of each spectrum at higher temperature such as 35 °C (Figure S7). However, at 35 °C, the considerable portion (ca. 40%) of the initial $\mathbf{TBA}^{(5,8)\mathbf{NB2}}$. $\mathbf{CS}^{(5,8)\mathbf{G7T}}$ duplex would dissociate into two unfolded single-stranded structures judging from its UV thermal melting curve. The CD spectral change at 25 °C is also presented in Figure S8, which shows the smaller change compared with that at 30 °C. Thereby, temperature near 30 °C would be optimal conditions to induce structural transition from duplex to quadruplex as large as possible in this system.

(27) Markham, N. R.; Zuker, M. DINAMelt web server for nucleic acid melting prediction. *Nucleic Acids Res.* **2005**, *33*, W577−W581.

(28) (a) Alberti, P.; Mergny, J.-L. DNA duplex−quadruplex exchange as the basis for a nanomolecular machine. *Proc. Natl. Acad. Sci. U.S.A.* **2003**, *100*, 1569−1573. (b) Uno, S.-n.; Dohno, C.; Bittermann, H.; Malinovskii, V. L.; Häner, R.; Nakatani, K. A light-driven supramolecular optical switch. *Angew. Chem., Int. Ed.* **2009**, *48*, 7362−7365. For reviews (c) Beissenhirtz, M. K.; Willner, I. DNA-based machines. *Org. Biomol. Chem.* **2006**, *4*, 3392−3401. (d) Seeman, N. C. From genes to machines: DNA nanomechanical devices. *Trends Biochem. Sci.* **2005**, *30*, 119−125. (e) Krishnan, Y.; Simmel, F. C. Nucleic acid based molecular devices. *Angew. Chem., Int. Ed.* **2011**, *50*, 3124−3156.

(29) (a) Yurke, B.; Turberfield, A. J.; Mills, A. P., Jr.; Simmel, F. C.; Neumann, J. L. A DNA-fuelled molecular machine made of DNA. *Nature* **2000**, *406*, 605−608. For review (b) Zhang, D. Y.; Seelig, G. Dynamic DNA nanotechnology using strand-displacement reactions. *Nat. Chem.* **2011**, *3*, 103−113.

(30) Miyoshi, D.; Matsumura, S.; Nakano, S.-i.; Sugimoto, N. Duplex dissociation of telomere DNAs induced by molecular crowding. *J. Am. Chem. Soc.* **2004**, *126*, 165−169.

(31) Fadock, K. L.; Manderville, R. A.; Sharma, P.; Wetmore, S. D. Optimization of fluorescent 8-heteroaryl-guanine probes for monitoring protein-mediated duplex→G-quadruplex exchange. *Org. Biomol. Chem.* **2016**, *14*, 4409−4419.

(32) Wang, X.; Huang, J.; Zhou, Y.; Yan, S.; Weng, X.; Wu, X.; Deng, M.; Zhou, X. Conformational switching of G-quadruplex DNA by photoregulation. *Angew. Chem., Int. Ed.* **2010**, *49*, 5305−5309.

(33) Liu, D.; Bruckbauer, A.; Abell, C.; Balasubramanian, S.; Kang, D.-J.; Klenerman, D.; Zhou, D. A reversible pH-driven DNA nanoswitch array. *J. Am. Chem. Soc.* **2006**, *128*, 2067−2071.

(34) (a) Ikeda, M.; Tanida, T.; Yoshii, T.; Kurotani, K.; Onogi, S.; Urayama, K.; Hamachi, I. Installing logic-gate responses to a variety of biological substances in supramolecular hydrogel−enzyme hybrids. *Nat. Chem.* **2014**, *6*, 511−518. (b) Shigemitsu, H.; Fujisaku, T.; Onogi, S.; Yoshii, T.; Ikeda, M.; Hamachi, I. Preparation of supramolecular hydrogel−enzyme hybrids exhibiting biomolecule-responsive gel degradation. *Nat. Protoc.* **2016**, *11*, 1744−1756.



DOI: 10.1021/acsomega.8b01177
*ACS Omega* 2018, 3, 9267−9275